ACS APPLIED MATERIALS & INTERFACES

Research Article

www.acsami.org

Substrate Biasing Effect on the Physical Properties of Reactive RF-Magnetron-Sputtered Aluminum Oxide Dielectric Films on ITO Glasses

Ling Yan Liang,* Hong Tao Cao,* Quan Liu, Ke Min Jiang, Zhi Min Liu, Fei Zhuge, and Fu Ling Deng

Division of Functional Materials and Nano Devices, Ningbo Institute of Material Technology and Engineering, Chinese Academy of Sciences, Ningbo 315201, People's Republic of China

Supporting Information

ABSTRACT: High dielectric constant (high-k) Al_2O_3 thin films were prepared on ITO glasses by reactive RF-magnetron sputtering at room temperature. The effect of substrate bias on the subband structural, morphological, electrode/Al_2O_3 interfacial and electrical properties of the Al_2O_3 films is systematically investigated. An optical method based on spectroscopic ellipsometry measurement and modeling is adopted to probe the subband electronic structure, which facilitates us to vividly understand the band-tail and deep-level (4.8−5.0 eV above the valence band maximum) trap states. Well-selected substrate biases can suppress both the trap states due to promoted migration of sputtered particles, which optimizes the leakage current density, breakdown strength, and quadratic voltage coefficient of capacitance. Moreover, high porosity in the unbiased Al_2O_3 film is considered to induce the absorption of atmospheric moisture and the consequent occurrence of electrolysis reactions at electrode/Al_2O_3 interface, as a result ruining the electrical properties.

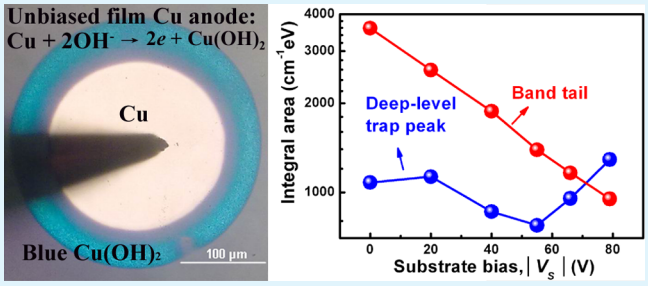

KEYWORDS: *Al_2O_3 thin films, magnetron sputtering, leakage current, breakdown mechanism, oxygen vacancy, subband electronic structure*

INTRODUCTION

Considerable efforts have been devoted to high-dielectric constant (high-k) materials during the past decade, for the applications such as thin film transistor, high electron mobility transistor, and dynamic random access memory, in which high-k material is required to possess high dielectric constant, low leakage current, and high breakdown strength.[1−3] Binary metal oxides, such as Al_2O_3, Ta_2O_5, HfO_2, Y_2O_3, and ZrO_2, have been intensively investigated for the above-mentioned applications.[4,5] Among them, Al_2O_3 is of great interest because of its abundance in nature, low-cost, good chemical stability, and robust physical properties.[2,6,7]

Recently, high-k oxides including Al_2O_3 fabricated on transparent and/or flexible conductive substrates have been gaining ever-increasing attentions because of their applications in transparent electronics and flexible electronics.[8−10] It is highly desirable to deposit high-k thin films with low temperature, which facilitates practical applications of large area, low-cost plastic or glass substrates. Al_2O_3 thin films have been prepared by various methods such as electrochemical anodization,[11] sol−gel deposition,[12] spray pyrolysis,[13] thermal oxidation of Al or AlN films,[14,15] plasma oxidation of Al films,[16] plasma arc deposition,[17] chemical vapor deposition,[18] atomic layer deposition,[10] and magnetron sputtering.[19,20] Among them, magnetron sputtering has the advantage of the preparation of large-area uniform films with relatively high growth rate even at low deposition temperatures for large-scale industrial application.[5] In particular, the substrate biasing-assisted sputtering process can offer a new degree of freedom to tune the film properties more subtly.[3] Huang A. P. et al. and Brassard D. et al. have reported on the effect of substrate bias on the properties of sputtered high-k films (such as $Ti_xSi_{1-x}O_2$, Ta_2O_5) on Si substrates.[3,21] A small bias was found to densify the ternary $Ti_xSi_{1-x}O_2$ films because of the beneficial "soft-hammering" effect and then improve the electrical properties of the films, but nevertheless higher biases caused the enrichment of Ti in the films and creation of structural defects.[3] For Ta_2O_5 thin films, a monotonous improvement of the electrical properties with increasing substrate bias voltage was observed that was derived from the substrate bias-induced crystallization effect.[21]

There were reports on the influence of oxygen partial pressure, total working pressure, and sputtering power upon the electrical properties of Al_2O_3 thin films grown on ITO glasses.[19,22] It revealed that it is a challenge to grow high-quality dielectric films at low temperatures by magnetron

Received: June 9, 2013
Accepted: February 3, 2014
Published: February 3, 2014

Table 1. Lorentz Parameter Values for Fitting the Optical Functions of the Al_2O_3 films with Different Substrate Bias Voltages (V_S)[a]

	V_S (V)					
	0	−20	−40	−55	−66	−79
t (nm)	154.8	151.8	151.8	154.9	151.4	153.0
A_1	0.00594	0.00770	0.00683	0.00661	0.00673	0.0129
E_{01} (eV)	4.82	5.00	5.03	4.91	4.97	5.01
A_2	1.777	2.335	9.315	8.473	14.93	12.14
E_{02} (eV)	6.96	7.24	7.24	7.16	7.17	7.23
MSE	9.212	6.585	5.098	5.354	4.957	4.271

[a]The subscripts 1 and 2 stand for the first and second Lorentz function, respectively. t and MSE are the Al_2O_3 film thickness and mean-squared error, respectively.

sputtering on the plastics or ITO glass substrates with rough surface. Recent investigation has suggested that the sputtering of thin film on different substrates is a complicated process involving chemical interaction, physical nucleation and diffusion, and thin film growth.[23,24] Voigt et al. had reported that, the so-called shadowing effect can result in self-enhanced roughening of the surface during the deposition since the surface diffusion constant is relatively small at a low substrate temperature, and the rough surface of the substrate can further promote the shadowing effect and increase the surface roughness of the upper films.[19] In addition, the electrical properties could be seriously affected by various defects such as oxygen vacancies and interstitial oxygen,[25] which are inevitably generated during the low-temperature sputtering process. Could substrate bias make a positive contribution to solve those problems? Therefore the effect of the substrate bias on the electrical properties of Al_2O_3 thin films is required a comprehensive clarification.

In this work, we systematically investigate the effect of substrate bias voltage on the subband structural, surface morphological, electrode/Al_2O_3 interfacial and electrical properties of Al_2O_3 thin films. Particularly, we apply an optical method to detect the subband absorption, in order to grasp the electronic subband structure (including the band-tail and the deep-level trap states). The results demonstrated that, the leakage currents, the frequency and voltage dependence of the dielectric property are significantly reduced by applying a moderate bias voltage, and the correlations among the electrical properties, film density, surface morphology, and the band-tail and deep-level trap states are tightly coupled.

EXPERIMENTAL SECTION

The Al_2O_3 thin films were grown on ITO glass substrates by a reactive RF (13.56 MHz) magnetron sputtering system with a 2 in.-diameter aluminum target (99.9% purity) at a power of 100 W. The sputtering deposition process was performed at a chamber pressure of 0.24 Pa maintaining an argon-to-oxygen ration of 7/1. Aluminum target was presputtered in a pure argon atmosphere for 10 min before deposition, in order to get rid of the contaminations on the target surface. The substrate bias voltage was controlled by an independent RF-power (13.56 MHz) source. The direct current (DC) substrate bias voltage (V_s) is defined here as the negative DC potential when the bias RF power is applied. In this case, argon ions would bombard the surface of the growing film, and the bombardment strength could be controlled by V_s. The DC substrate bias voltages were scanned from 0 to −79 V (the corresponding RF power in the range from 0 to 80 W). The in situ substrate heating and postannealing were unintentionally carried out in this study.

For the dielectric characterizations of the sputtered Al_2O_3 films, Cu/Al_2O_3/ITO MIM capacitors were fabricated. Cu (100 nm) top electrodes were deposited by electron beam evaporation through a shadow mask with a contact area of 3.14×10^{-4} cm^2. The capacitors were analyzed by capacitance−voltage (C−V) and current density−voltage (J−V) measurements using an HP4284A precision LCR meter and a precision semiconductor analyzer (Keithley 4200) in the dark at room temperature, respectively. The thickness, porosity and subband absorption properties of the films were characterized by a variable angle spectroscopic ellipsometer (J.A.Woollam Co., Inc.) in the UV−vis−NIR range. The morphology of the films and ITO glass substrate was investigated through atomic force microscopy (AFM, Veeco Dimention V) measurement. The chemical components of the films are detected by X-ray photoelectron spectroscopy (XPS, Kratos Analytical Ltd., UK) equipped with a standard monochromatic Al-K_α source (1486.6 eV). High dose of argon ions (2 KV) was used to sputter away the top hydrated and carbon contamination layer (4−5 nm) of the films. Microarea XPS analyses were also carried out by applying a circular X-ray beam with 110 μm in diameter, in order to study the chemical evolution of Cu at the Cu/Al_2O_3 interface. The binding energy data were calibrated with respect to the C1s signal of ambient hydrocarbons (C−H and C−C) at 284.8 eV.

RESULTS AND DISCUSSION

Subband Absorption and Porosity. In this section, the electronic subband structure and the porosity of aluminum oxide films are analyzed by means of the spectroscopic ellipsometry (SE) measurement in the UV−vis−NIR range from 0.73 to 6.2 eV. The ellipsometric angle ψ and phase difference Δ were recorded at incidence angles of 55, 65, and 75°, respectively. The SE spectra were analyzed by a simple three-phase model consisting of substrate/Al_2O_3/surface rough layer (50% Al_2O_3 + 50% void). In this model, unknown parameters of film thickness and dielectric constant for Al_2O_3 films are designated as fitting variables.

Considering the wide bandgap of Al_2O_3, Cauchy dispersion model combined with Urbach tail relation usually used for transparent films was adopted to acquire the dielectric function of the Al_2O_3 film in the range of 0.73−6.2 eV (The spectroscopic ellipsometry data and fitted curves are available in the Supporting Information). However, the mean-squared error (MSE) values, as the criteria to evaluate to fitting quality, are beyond 20 (Generally, the fitting quality is acceptable if the MSE value is less than 10). Therefore, the absorption related to defect states is unneglectable, so the Cauchy & Urbach tail model is incompetent in our case. Consequently, we employed the Lorentz oscillator model to represent the dielectric function ($\varepsilon(h\upsilon)$) of the aluminum oxide films, described as follows

$$\varepsilon(h\upsilon) = \varepsilon_1 + i\varepsilon_2 = \sum_j \frac{A_j}{E_{0j}^2 - (h\upsilon)^2 - iB_j h\upsilon} \quad (1)$$

where A_j, E_{0j}, and B_j are the amplitude, center energy and damping coefficient of each oscillator in eV, respectively. Two oscillators are used in the data analysis and the key parameters are listed in Table 1. A good agreement between the experimental and fitting spectra is obtained over the studied range for all the films (seen in the Supporting Information), as confirmed that all the MSE values are below 10, implying that the Lorentz oscillator model is applicable in this study.

In Table 1, the oscillator center energies E_{01} and E_{02} for all the samples converge to 4.97 and 7.17, respectively. The E_{01} value is far below the bandgap energy of aluminum oxide. It is speculated that the oscillator at 4.97 eV is related to the oxygen defects. Based on the previous calculation,[25] the 0/− level of oxygen vacancy in amorphous aluminum oxide is located at 4.8 eV above the valence band edge, which is close to E_{01}. Therefore, the oscillator at 4.97 eV can be assigned to the transition from the valence band to the oxygen vacancy-related defect level. The E_{02} value is in between the theoretical bandgap energies of amorphous (6.2−6.5 eV) and bulk (8.8 eV) aluminum oxide,[25] indicating that the oscillator at 7.17 eV is corresponding to the bandgap transition of our aluminum oxide films.

The refractive index n_f and extinction coefficient k_f can be calculated from the dielectric function by

$$n_f = \left[\frac{1}{2}\sqrt{\varepsilon_1^2 + \varepsilon_2^2} + \varepsilon_1\right]^{1/2}$$
$$k_f = \left[\frac{1}{2}\sqrt{\varepsilon_1^2 + \varepsilon_2^2} - \varepsilon_1\right]^{1/2} \quad (2)$$

The optical absorption coefficients α_{opt} can be obtained via $\alpha_{opt} = 4\pi k_f/\lambda$, as depicted in Figure 1a. The absorption spectra of all the films feature a peak and a band tail, as displayed in the insert of Figure 1a. The band tails can be fitted by the exponential law, i.e., the so-called Urbach tail expressed by[26]

$$\alpha_{opt} = \alpha_0 \exp\left(\frac{h\upsilon - E_1}{E_0}\right) \quad (3)$$

Here α_0 is an absorption parameter, E_1 a certain energy of the order of the band gap, and E_0 an empirical parameter describing the width of the localized states in the bandgap. The Urbach tail below the fundamental absorption edge is usually observed due to the disorder structure of the amorphous network. The peak is believed to originate from the oxygen vacancy-induced optical absorption since the peak position is calculated to be assigned to E_{01}. Interestingly, the peak integral area is found to be proportional to the density of the oxygen vacancy N_t, because the defect-induced absorption coefficient $\alpha_{defects}$ can be expressed in terms of N_t as[27]

$$\alpha_{defects} = N_t S f_i (1 - f_f) \quad (4)$$

where S is the optical absorption parameter per defect, while f_i and f_f are the occupation probabilities of electrons in the initial and final states, respectively.

The integral areas of the band tail- and peak-assigned components are respectively calculated, as highlighted in Figure 1b. The band tail area decreases with increasing bias voltages, indicating that the band-tail states near the absorption edge are gradually diminished. The deposited atoms under a substrate bias have high kinetic energy enough to diffuse more freely on the film surface so as to occupy or approach the equilibrium

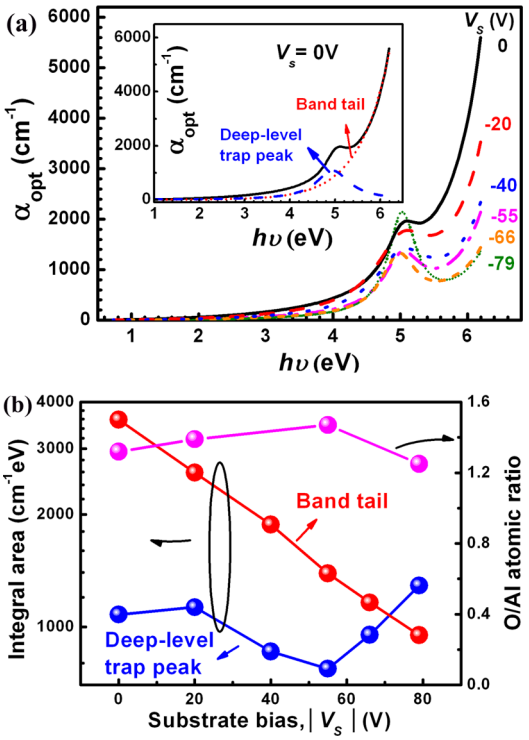

Figure 1. (a) Absorption coefficient α of the Al_2O_3 films with $|V_s| = 0$−79 V. The insert gives an example that the absorption spectrum can be deconvoluted into a band tail and a peak. (b) The integral areas of the band tail and deep-level trap peak as a function of substrate bias voltage$|V_s|$. The O/Al atomic ratios of the typical films are also shown.

lattice position, which resultantly decreases the degree of disorder in the sputtered Al_2O_3 thin films. The peak area that represents the density of oxygen vacancies, decreases first and then increases, showing the minimum value at $V_s = -55$ V. The decreasing trend of the oxygen vacancy density is believed to be a result of the beneficial effect of ion bombardment. But nevertheless, further increase of the substrate bias voltage ($|V_S| > 55$ V) is found to be accompanied with the rebound of the oxygen vacancies. The most possible reason is that the excessive energetic Ar ion bombardment brings about preferential resputtering of oxygen in the films, which promotes the formation of more oxygen vacancies. The O/Al atomic ratio calculated according to XPS spectra (the XPS spectra of typical films are available in the Supporting Information), increases first and then decreases, showing the maximum value (~1.47) at $V_s = -55$ V, as displayed in Figure 1b. This evolution is self-consistent with the variation of oxygen vacancies, indicating that the optical method based on SE measurement and analysis is feasible to probe the subband electronic structure of oxide films.

The refractive index n_f at a wavelength of 550 nm is plotted as a function of V_s in Figure 2a. The refractive index is the indicator of the packing density of the films, since the volume fraction of porosity p of each film can be deduced by the following formula[28]

$$p = 1 - (n_f^2 - 1)/(n_b^2 - 1) \quad (5)$$

where n_b is the refractive index of bulk Al_2O_3. As $|V_S|$ is increased from 0 to 20 V, the porosity is found to decrease significantly from ~15% to 10%, as manifested in Figure 2b. Then, it increases slowly until reaches to ~12% at $V_s = -79$ V.

dx.doi.org/10.1021/am4055589 | ACS Appl. Mater. Interfaces 2014, 6, 2255−2261

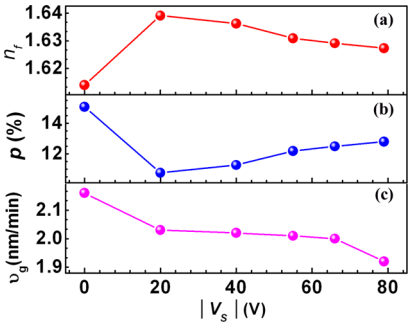

Figure 2. Refractive index (a) n_f, (b) porosity p, and (c) growth rate υ_g of the Al_2O_3 films as a function of substrate bias voltage.

The porosity evolution of the films manifests that, the proper ion bombardment favors growing more densely packed films as reported in ref 3, whereas excessive energy ion bombardment would reduce the packing density, revealed by the fact that the porosity of the film with the largest bias voltage is lower than that of the unbiased one.

The thickness (t) of the films deposited at various V_s is maintained around 150 nm by altering the growth time. Figure 2c illustrates the variation of the mean growth rate (V_g) as a function of V_s. It is evident that the overall trend of the growth rate is decreasing when the V_s is applied, which is believed to be a result of whether the densification of the films or the occurrence of resputtering, especially preferential oxygen resputtering that is well-known for oxides.[3,29] The latter one might induce the increase of oxygen vacancy, demonstrated by the increased area of the peak assigned to oxygen vacancy.

Morphological Characteristics. The morphological features of the Al_2O_3 thin films were examined by AFM. Figure 3a–c illustrate the representative surface morphologies of the

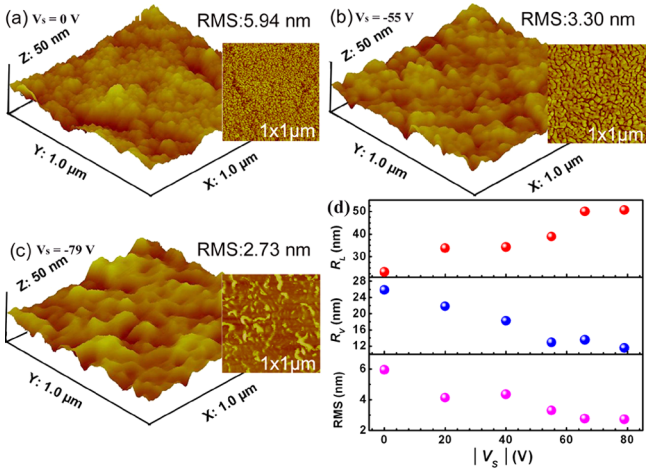

Figure 3. Three dimensional view of 1 × 1 μm^2 morphologies for the Al_2O_3 films by AFM at (a) V_s = 0 V, (b) V_s = −55 V, (c) V_s= −79 V. The inset is the phase image. (d) The mean lateral size (R_L), vertical size (R_V) and RMS roughness obtained from AFM observations for the Al_2O_3 films with $|V_s|$ = 0–79 V.

Al_2O_3 thin films deposited at various V_s. The unbiased film has a relatively rough surface with some valleys and small spherical agglomerates. Its root-mean-square (RMS) roughness (5.94) is higher than that of the ITO glass substrate (3.99 nm) due to self-enhanced roughening of the surface during the deposition. Fortunately, the applying of substrate bias effectively modified the surface morphology, as seen the agglomerates grow up along the surface but collapse in the vertical direction. The mean lateral and vertical size can be extracted from the phase images, as shown in Figure 3d. Along with the disappearance of the so-called profile valleys, the RMS roughness shows an obvious reduction from 5.94 to 2.73 nm as V_s changed from 0 to −79 V. The surface smoothening effect is also attributed to the ion bombardment for which the arriving adatoms can diffuse more freely on the film surface.

Special Phenomena Occurring at the Electrode/Dielectric Interface. During the electrical measurement for the aluminum oxide films without applying substrate bias, it was observed that, the color at the margin of the Cu electrode became bright blue (see Figure 4a) when a modest positive

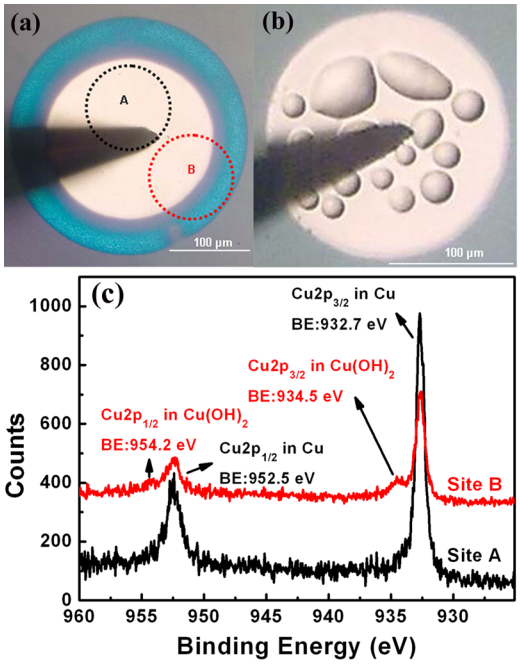

Figure 4. Optical microscope pictures of Cu electrodes on the unbiased film after (a) positive measurement bias and (b) negative measurement bias. (c) Cu 2p XPS spectra of the Cu electrode at sites A and B in a.

voltage (>15 V) was applied on the Cu electrode for several tens of seconds. It is speculated that the bright blue color comes from the formation of $Cu(OH)_2$, which was confirmed by XPS measurements. Figure 4c displays the Cu 2p spectra obtained from the center (labeled with A in Figure 4a) and margin (labeled with B in Figure 4a) area of the Cu electrode, respectively. The Cu 2p spectrum from site A shows two peaks located at 952.5 and 932.7 eV, which are corresponding to the $2p_{1/2}$ and $2p_{3/2}$ features of the metallic Cu, respectively. Except these two peaks, however, two new peaks centered at 954.2 and 934.5 eV in the Cu 2p spectrum from site B were stretched out, which respectively correspond to the Cu $2p_{1/2}$ and Cu $2p_{3/2}$ of $Cu(OH)_2$.[30,31] Moreover, bubble-shaped embossment emerged one by one on the Cu electrode when a modest negative voltage was applied on the Cu electrode (see Figure 4b). In contrast, however, the above phenomena are not observed for the aluminum oxide films deposited with substrate biases.

Based on the above analysis, it is believed that electrolysis reactions happened at the Cu/Al_2O_3 interface during the

dx.doi.org/10.1021/am4055589 | ACS Appl. Mater. Interfaces 2014, 6, 2255–2261

electrical measurement. The reactions can be described as follows

$$Cu + 2OH^- \rightarrow 2e + Cu(OH)_2 \text{ (when the Cu electrode serves as the anode)} \quad (6)$$

$$2H^+ + 2e \rightarrow H_2 \uparrow \text{ (when the Cu electrode serves as the cathode)} \quad (7)$$

These reaction formulas are capable of explaining the experimental observations (bright blue color and bubble-shaped embossment formation) very well. The electrolysis reactions imply that a lot of absorbed moisture is present on the surface or even in the bulk of the unbiased aluminum oxide film, because it has a rough surface and a high porosity. This is proved by the detection of absorbed water in the unbiased film by XPS measurement (seen in the Supporting Information). In contrast, the similar phenomena were not observed for the substrate biased aluminum oxide films, which correlates well with the smooth surface and densification effect revealed by AFM and SE measurements.

Electrical Properties. Figure 5a represents the leakage current density vs. applied electric field (J-E) characteristics

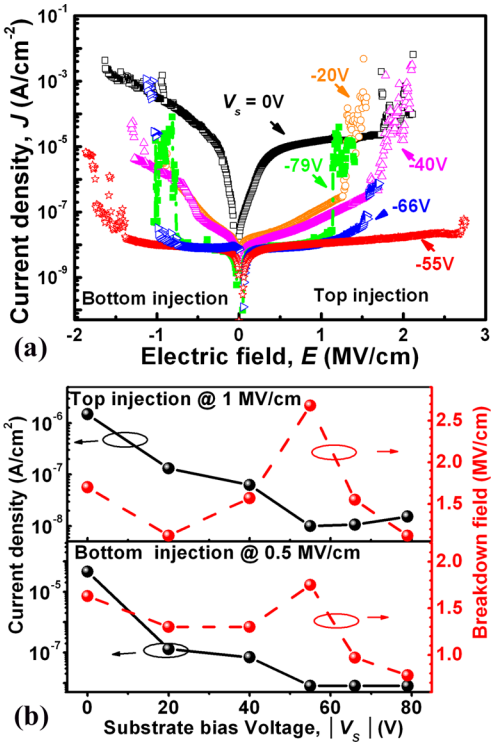

Figure 5. (a) J–V curves of Cu/Al_2O_3/ITO capacitors at different substrate bias voltages. (b) Leakage current density and breakdown field of the Al_2O_3 films as a function of substrate bias voltage.

under both top injection (electron injection from the top electrode) and bottom injection modes. For clarity, the leakage current density and the breakdown field strength are plotted as a function of V_s in Figures 5b. For the unbiased films, the asymmetry of leakage current for the top injection (1.5×10^{-5} A/cm^2 @ 1 MV/cm) and bottom injection mode (2×10^{-4} A/cm^2 @ 1 MV/cm) is due to the asymmetrical electrode utilized. When a small substrate bias ($V_s \approx -20$ V) is applied during the film growth, the leakage current is found to be suppressed significantly. At $V_s = -55$ V, the leakage current is reduced as low as around 1×10^{-8} A/cm^2 at 1 MV/cm. Then afterward a further increase of V_s is found to be accompanied with a little deterioration of the leakage current. Moreover, the biggest breakdown field strength (~ 2.7 MV/cm and ~1.8 MV/cm for the top and bottom injection mode, respectively) is also obtained at $V_s = -55$ V. The breakdown field strength of sputtered Al_2O_3 thin films (<300 nm) reported in the literatures is ranging from 2 to 5 MV/cm.[19] The usage of Cu instead of Al as the electrode material can reduce the breakdown field strength, as formerly observed by Yip et al.[2] They reported that the Al/Al_2O_3/Al capacitors display a breakdown field strength beyond 4 MV/cm, while that of the Al/Al_2O_3/Cu capacitors is less than 1.5 MV/cm, which is comparable to the value of our Cu/Al_2O_3/ITO capacitors.

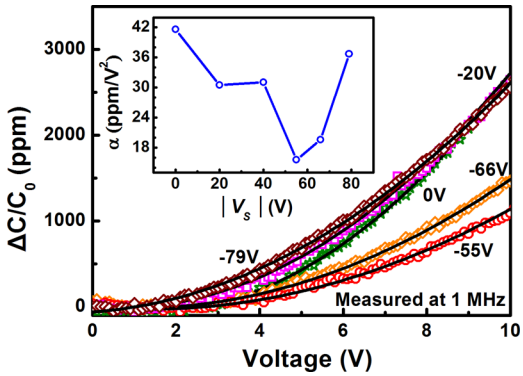

Figure 6. $\Delta C/C_0$–V characteristics of sputtered Al_2O_3 thin films at various substrate bias voltages. The inset plots the quadratic voltage coefficient α of capacitance as a function of substrate bias voltage $|V_s|$.

The normalized capacitance density vs. applied voltage ($\Delta C/C_0$–V), shown in Figure 6, can be obtained by fitting the measured data with a second-order polynomial equation[32]

$$\Delta C(V) = C_0(\alpha V^2 + \beta V) \quad (8)$$

where C_0 is the capacitance density at $V = 0$ V, whereas α and β represent the quadratic and linear voltage coefficients of capacitance, respectively. Since the linear voltage coefficient (VCC-β) can be reduced to zero by appropriate circuit design, VCC-α is the most important MIM capacitor parameter for analogue circuit applications.[32] The film deposited at $V_s = -55$ V exhibits the smallest VCC-α of ~15.6 ppm/V^2 at $C_0 = 0.51$ fF/μm^2, as seen in the inset of Figure 6, It is reported that TaN/Al_2O_3/TaN capacitors on Si wafer show a VCC-α of ~795 ppm/V^2 at $C_0 = 6.05$ fF/μm^2.[33] Considering that VCC-α generally increases linearly with $1/t^2$ (i.e.,C_0^2 for the same material),[34] the VCC-α value of our Cu/Al_2O_3/ITO capacitors is a little higher, partly because of the relatively rough ITO electrodes.

The dielectric constant (k) of the Al_2O_3 thin films was evaluated from C_0 and shown in Figure 7. The dielectric constant of the fabricated Al_2O_3 varies between 8.8 and 10, in accordance with the pervious reports.[7,19] It is seen that the V_s has limited effect on the dielectric constant. However, the dielectric dispersion was reduced significantly by applying V_s, which is evident from the fact that the variation of dielectric constant in the operating frequency range (100 Hz to 1 MHz)

dx.doi.org/10.1021/am4055589 | ACS Appl. Mater. Interfaces 2014, 6, 2255–2261

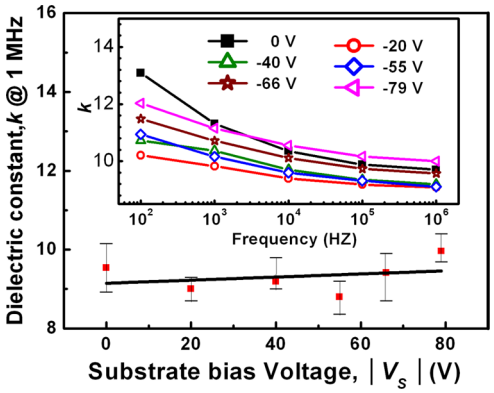

Figure 7. Effect of substrate bias voltage on the dielectric constant. The inset shows the frequency dependence of the dielectric constant.

is changed from ~26% for the films without substrate bias to 12−14% for the biased ones (see the inset of Figure 7).The film deposited at V_s = −55 V shows a dielectric constant of ~8.8, and an acceptable frequency dispersion of ~13%. Taken the leakage current density, breakdown field strength, VCC-α, dielectric constant and dielectric dispersion into considerations, the Al_2O_3 film deposited at V_s = −55 V has the optimal electrical performance in this study.

DISCUSSION

The subband structure, morphology, and interface studies of the films offer a deep insight into understanding the effect of the substrate bias voltage on their electrical properties.

When applying a substrate bias around −20 V, the leakage current is greatly improved. In fact, the films with larger porosity have more pores and microvoids in the films,[3] which facilitate absorbing the moisture in the air (proved by XPS measurement, as seen in the Supporting Information) to trigger the electrolysis reactions (Figure 4). The electrolysis reactions at the electrode/dielectric interface inevitably involve chaotic charge transfer at the interface, which is in line with the large leakage current of the unbiased aluminum oxide films (around 2 orders of magnitude higher than the −20 V-biased films, as seen in figure 5).

As $|V_S|$ increased from 20 to 55 V, the film leakage current decreases by about 1 order of magnitude, and the breakdown field strength are remarkably improved, in accordance with the variations of the subband trap density and the film surface roughness (Figures 1 and 3). The repair of oxygen vacancies and attenuation of band-tail defects would cause the improvement of the electrical properties. In fact, oxygen vacancies can drastically govern the electrical properties of dielectric oxides;[25] whereas the accumulation of band-tail states can narrow the band gaps[35] and reduce the band offsets between the electrode and dielectric oxide, and as a result boost the leakage current. Furthermore, the pristine smooth surface of the Al_2O_3 films favors to form a sound electrode/oxide interface, giving rise to the improvement of the electrical properties of the MIM capacitor.

Upon higher substrate bias voltage ($|V_S|$ > 55 V), however, it is found that both the breakdown field strength and the quadratic voltage coefficient of capacitance (VCC-α) are getting degenerated. The actual mechanism of the destructive breakdown is rather complicated. Nevertheless, the dielectric breakdown mechanism can be roughly classified into the intrinsic breakdown model and the extrinsic or defect-related breakdown section.[36] The intrinsic breakdown mechanism is hard to capture, provided only that all the extraneous variables have been isolated.[37] The breakdown phenomenon in the real experiment undoubtedly belongs to the defect-related process. The accumulation of oxygen vacancies is one of the most possible explanations for the degradation of the breakdown field strength. In addition, the VCC-α value is getting bigger along with the increase of the oxygen vacancies, just acting as a hint to describe the amount of deep traps.[34]

CONCLUSION

In this work, the subband structural, morphological, and electrode/Al_2O_3 interfacial properties of room-temperature sputtered Al_2O_3 thin films on ITO glasses were comprehensively investigated, in hope of in-depth understanding the effect of the substrate bias voltage on the electrical properties. The subband electronic structure, deduced by the optical method, could be divided into the band-tail state and deep-level trap state, in which the deep-level one was assigned to the oxygen vacancy due to its energy level (4.8−5.0 eV above the valence band maximum). The decrease of subband defects was found to be in line with the improvement of the leakage current density and breakdown field strength, while the rebound of oxygen vacancies under higher voltage bias negatively contributed to the breakdown field strength and quadratic voltage coefficient of capacitance. In addition, electrolysis reactions were demonstrated at the Cu electrode/unbiased-Al_2O_3 interface, which mainly accounts for the big leakage current density of the unbiased films. Under the optimal substrate bias (approximately −55 V), the room-temperature deposited Al_2O_3 thin films on ITO glasses were found to exhibit competitive electrical properties, i.e., a dielectric constant about 8.8 with small dielectric dispersion (~13%) and quadratic voltage coefficient (15.6 ppm/V^2) of capacitance, a leakage current as low as 1×10^{-8} A/cm^2 at 1 MV/cm, and a breakdown field strength higher than 2.7 MV/cm. It is suggested that one can take the advantage of the substrate biasing to improve the electrical properties of the Al_2O_3 gate dielectrics, which paves the way to realizing low-temperature-processed high-k dielectrics for transparent electronic applications.

ASSOCIATED CONTENT

Supporting Information

Spectroscopic ellipsometry data and fitted curves respectively using the Cauchy & Urbach tail model and the Lorentz model (Figure S1). The O 1s and Al 2p XPS spectra of typical Al_2O_3 thin films (Figure S2). This material is available free of charge via the Internet at http://pubs.acs.org.

AUTHOR INFORMATION

Corresponding Authors

*E-mail: h_cao@nimte.ac.cn.
*E-mail: lly@nimte.ac.cn.

Notes

The authors declare no competing financial interest.

ACKNOWLEDGMENTS

This work is supported by the Chinese National Program on Key Basic Research Project (2012CB933003), the National Natural Science Foundation of China (Grants 11104289 and 61274095), the Science and Technology Innovative Research Team of Ningbo Municipality (2009B21005), the Key Program

for Science and Technology Innovative Team of Zhejiang Province (2010R50020), and Analysis Research for Public Welfare Project of Zhejiang Province (2012C37047).

REFERENCES

(1) He, G.; Sun, Z. Q.; Li, G.; Zhang, L. D. Review and Perspective of Hf-based High-k Gate Dielectrics on Silicon. *Crit. Rev. Solid State Mater. Sci.* **2012**, *37*, 131−157.
(2) Yip, G.; Qiu, J.; Ng, W. T.; Lu, Z. H. Effect of Metal Contacts on the Electrical Characteristics of Al_2O_3 Dielectric Thin Films. *Appl. Phys. Lett.* **2008**, *92*, 122911.
(3) Brassard, D.; El Khakani, M. A.; Ouellet, L. Substrate Biasing Effect on the Electrical Properties of Magnetron-Sputtered High-k Titanium Silicate Thin Films. *J. Appl. Phys.* **2007**, *102*, 034106.
(4) Robertson, J. High Dielectric Constant Oxides. *Eur. Phys. J.: Appl. Phys.* **2004**, *28*, 265−291.
(5) Cang, K.; Liang, L. Y.; Liu, Z. M.; Wu, L.; Luo, H.; Cao, H. T.; Zou, Y. S. Influence of the Substrate Bias Voltage on the Physical Properties of dc Reactive Sputtered Ta_2O_5 Films. *J. Alloys Compd.* **2013**, *550*, 258−262.
(6) Mornida, H.; Hamada, T.; Takagi, Y.; Yamamoto, T.; Uda, T.; Ohno, T. Theoretical Study on Dielectric Response of Amorphous Alumina. *Phys. Rew. B* **2006**, *73*, 054108.
(7) Zhang, L.; Jiang, H. C.; Liu, C.; Dong, J. W.; Chow, P. Annealing of Al_2O_3 Thin Films Prepared by Atomic Layer Deposition. *J. Phys. D: Appl. Phys.* **2007**, *40*, 3707.
(8) Wager, J. F. Transparent Electronics. *Science* **2003**, *300*, 1245−1246.
(9) Meena, J. S.; Chu, M. C.; Kuo, S. W.; Chang, F. C.; Ko, F. H. Improved Reliability from A Plasma-Assisted Metal-Insulator-Metal Capacitor Comprising a High-k HfO_2 Film on A Fexible Polyimide Substrate. *Phys. Chem. Chem. Phys.* **2010**, *12*, 2582−2589.
(10) Munzenrieder, N.; Zysset, C.; Petti, L.; Kinkeldei, T.; Salvatore, G. A.; Troster, G. Flexible Double Gate a-IGZO TFT Fabricated on Free Standing Polyimide Foil. *Solid-State Electron.* **2013**, *84*, 198−204.
(11) Majewski, L. A.; Schroeder, R.; Grell, M. Flexible High Capacitance Gate Insulators for Organic Field Effect Transistors. *J. Phys. D: Appl. Phys.* **2004**, *37*, 21.
(12) Ortiz, A.; Alonso, J. C.; Pankov, V.; Huanosta, A.; Andrade, E. Characterization of Amorphous Aluminum Oxide Films Prepared by the Pyrosol Process. *Thin Solid Films* **2000**, *368*, 74−79.
(13) Aguilar-Frutis, M.; Garcia, M.; Falcony, C. Optical and Electrical Properties of Aluminum Oxide Films Deposited by Spray Pyrolysis. *Appl. Phys. Lett.* **1998**, *72*, 1700.
(14) Kolodzey, J.; Chowdhury, E. A.; Adam, T. N.; Qui, G.; Rau, I.; Olowolafe, J. O.; Suehle, J. S.; Chen, Y. Electrical Conduction and Dielectric Breakdown in Aluminum Oxide Insulators on Silicon. *IEEE Trans. Electron Devices* **2000**, *47*, 121−128.
(15) Taking, S.; MacFarlane, D.; Wasige, E. AlN/GaN MOS-HEMTs with Thermally Grown Al_2O_3 Passivation. . *IEEE Trans. Electron Devices* **2011**, *58*, 1418−1424.
(16) Ootomo, S.; Hashizume, T.; Hasegawa, H. A Novel Thin Al_2O_3 Gate Dielectric by ECR-Plasma Oxidation of Al for AlGaN/GaN Insulated Gate Heterostructure Field-Effect Transistors. *Phys. Status Solidi C* **2002**, *0*, 90−94.
(17) Schneider, J. M.; Larsson, K.; Lu, J.; Olsson, E.; Hjörvarsson, B. Role of Hydrogen for the Elastic Properties of Alumina Thin Films. *Appl. Phys. Lett.* **2002**, *80*, 1144.
(18) Koh, W.; Ku, S. J.; Kim, Y. Chemical Vapor Deposition of Al_2O_3 Films Using Highly Volatile Single Sources. *Thin Solid Films* **1997**, *304*, 222−224.
(19) Voigt, M.; Bergmaier, A.; Dollinger, G.; Sokolowski, M. Correlation of Chemical Composition and Electrical Properties of rf Sputtered Alumina Films. *J. Vac. Sci. Technol., A* **2009**, *27*, 234−244.
(20) Kakaki, H.; Pal, A. R.; Bailung, H.; Chutia, J. Effect of Oxygen on the Characteristics of Radio Frequency Planar Magnetron Sputtering Plasma Used for Aluminum Oxide Deposition. *J. Appl. Phys.* **2007**, *101*, 083304.
(21) Huang, A. P.; Chu, P. K. Improvement of Interfacial and Dielectric Properties of Sputtered Ta_2O_5 Thin Films by Substrate Biasing and the Underlying Mechanism. *J. Appl. Phys.* **2005**, *97*, 114106.
(22) Lee, J.; Kim, S. S.; Im, S. Electrical Properties of Aluminum Oxide Films Deposited on Indium-Tin-Oxide Glasses. *J. Vac. Sci. Technol., B* **2003**, *21*, 953−956.
(23) Schwartzkopf, M.; Buffet, A.; Körstgens, V.; Metwalli, E.; Schlage, K.; Benecke, G.; Perlich, J.; Rawolle, M.; Rothkirch, A.; Heidmann, B.; Herzog, G.; Müller-Buschbaum, P.; Röhlsberger, R.; Gehrke, R.; Stribeck, N.; Roth, S. V. From Atoms to Layers: In Situ Gold Cluster Growth Kinetics During Sputter Deposition. *Nanoscale* **2013**, *5*, 5053−5062.
(24) Yu, S.; Santoro, G.; Sarkar, K.; Dicke, B.; Wessels, P.; Bommel, S.; Döhrmann, R.; Perlich, J.; Kuhlmann, M.; Metwalli, E.; Risch, J. F. H.; Schwartzkopf, M.; Drescher, M.; Müller-Buschbaum, P.; Roth, S. V. Formation of Al Nanostructures on Alq3:An in Situ Grazing Incidence Small Angle X-ray Scattering Study during Radio Frequency Sputter Deposition. *J. Phys. Chem. Lett.* **2013**, *4*, 3170−3175.
(25) Liu, D.; Clark, S. J.; Robertson, J. Oxygen Vacancy Levels and Electron Transport in Al_2O_3. *Appl. Phys. Lett.* **2010**, *96*, 032905.
(26) Wasim, S. M.; Marin, G.; Rincón, C.; Sánchez Pérez, G.; Mora, A. E. Urbach's Tails in the Absorption Spectra of $CuInTe_2$ Single Crystals with Various Deviations from Stoichiometry. *J. Appl. Phys.* **1998**, *83*, 3318.
(27) Li, M. F. *Semiconductor Physics*, 1st ed.; Science Press: Beijing, 1991.
(28) Zhuo, H.; Peng, F. C.; Lin, L. M.; Qu, Y.; Lai, F. C. Optical Properties of Porous Anodic Aluminum Oxide Thin Films on Quartz Substrates. *Thin Solid Films* **2011**, *519*, 2308−2312.
(29) Yang, M. M.; Reith, T. M.; Lin, C. J. Process Effects on Radio Frequency Diode Reactively Sputtered ZrO_2 Films. *J. Vac. Sci. Technol., A* **1990**, *8*, 3925−3928.
(30) Morales, J.; Sánchez, L.; Martin, F.; Ramos-Barrado, J. R.; Sánchez, M. Use of Low-Temperature Nanostructured CuO Thin Films Deposited by Spray-Pyrolysis in Lithium Cells. *Thin Solid Films* **2005**, *474*, 133−140.
(31) Kerber, S. J.; Bruckner, J. J.; Wozniak, K.; Seal, S.; Hardcastle, S.; Barr, T. L. The Nature of Hydrogen in X-ray Photoelectron Spectroscopy: General Patterns from Hydroxides to Hydrogen Bonding. *J. Vac. Sci. Technol., A* **1996**, *14*, 1314−1320.
(32) Chang, K. C.; Huang, C. C.; Chen, G. L.; Chen, W. J.; Kao, H. L.; Wu, Y. H.; Chin, A.; McAlister, S. P. High-Performance $SrTiO_3$MIM Capacitors for Analog Applications. *IEEE Trans. Electron Devices* **2006**, *53*, 2312−2319.
(33) Ding, S. J.; Huang, Y. J.; Huang, Y.; Pan, S. H.; Zhang, W.; Wang, L. K. High density Al_2O_3/TaN-based metal−insulator−metal capacitors in application to radio frequency integrated circuits. *Chin. Phys. (Beijing, China)* **2007**, *16*, 2803−2806.
(34) Huang, C. C.; Cheng, C. H.; Liou, B. H.; Yeh, F. S.; Chin, A. Effect of Ta_2O_5 Doping on Electrical Characteristics of $SrTiO_3$ Metal-Insulator-Metal Capacitors. *J. Appl. Phys.* **2009**, *48*, 081401.
(35) Wang, X. J.; Zhang, L. D.; Zhang, J. P.; He, G.; Liu, M.; Zhu, L. Q. Effects of Post-Deposition Annealing on the Structure and Optical Properties of Y_2O_3 Thin Films. *Mater. Lett.* **2008**, *62*, 4235−4237.
(36) Verweij, J. F.; Klootwijk, J. H. Dielectric Breakdown I: A Review of Oxide Breakdown. *Microelectron. J.* **1996**, *27*, 611−622.
(37) O'Dwyer, J. J. Breakdown in Solid Dielectrics. *IEEE Trans. Electr. Insul.* **1982**, *17*, 484−487.